This is a preprint, the final version is subject to change, of the American Mineralogist (MSA)
Cite as Authors (Year) Title. American Mineralogist, in press.
(DOI will not work until issue is live.) DOI: http://dx.doi.org/10.2138/am-2017-5905

Revision 4

Shock-induced P-T conditions and formation mechanism of akimotoite-pyroxene glass assemblages in the Grove Mountains (GRV) 052082 (L6) meteorite

Lu Feng[1,2], Masaaki Miyahara[3,4], Toshiro Nagase[5], Eiji Ohtani[3], Sen Hu[1], Ahmed El Goresy[6], Yangting Lin[1*]

[1]Key Laboratory of Earth and Planetary Physics, Institute of Geology and Geophysics, Chinese Academy of Sciences, China.

[2]Guangzhou Institute of Geochemistry, Chinese Academy of Sciences, Guangzhou, China

[3]Institute of Mineralogy, Petrology, and Economic Geology, Tohoku University, Japan.

[4]Department of Earth and Planetary Systems Science, Graduate School of Science, Hiroshima University, Higashi-Hiroshima, 739-8526, Japan

[5]Center for Academic Resources and Archives, Tohoku University, Japan.

[6]Bayerisches Geoinstitut, Universität Bayreuth, 95447 Bayreuth, Germany.

[*]Corresponding author: LinYT@mail.igcas.ac.cn

Abstract: Akimotoite ((Mg,Fe)SiO_3-ilmenite) was encountered in shock-induced melt veins of Grove Mountains (GRV) 052082, a highly equilibrated low iron ordinary chondritic meteorite (L6). Coexistence of ringwoodite, majorite and majorite-pyrope solid solution indicates the shock pressure at 18-23 GPa and

temperature of 2000-2300 ºC during the natural dynamic event. Most low-Ca pyroxene clasts entrained in the melt veins have been partially or entirely transformed into akimotoite-pyroxene glass assemblages, which contain micron-sized areas with various brightness in the back-scattered electron images, different from the chemically homogeneous grains in the host-rock ($Fs_{20.5-21.3}$). The transmission electron microscopy study of a focused ion beam (FIB) slice from the heterogeneous areas shows that the assemblages are composed of FeO-depleted and heterogeneous akimotoite (Fs_{6-19}) crystals (100 nm up to 400 nm in size) scattered in FeO-enriched and relatively homogeneous pyroxene glass (Fs_{31-39}). All analyses of the akimotoite-pyroxene glass assemblages plot on a fractionation line in FeO-MgO diagram, with the host-rock pyroxene at the middle between the compositions of FeO-enriched akimotoite and the FeO-depleted pyroxene glass. These observations are different from previous reports of almost identical compositions of akimotoite, bridgmanite ($(Mg,Fe)SiO_3$-perovskite) or pyroxene glass to the host rock pyroxene (Chen et al., 2004; Ferroir et al., 2008; Ohtani et al., 2004; Tomioka and Fujino, 1997), which is consistent with solid-state transformation from pyroxene to akimotoite and preexisting bridgmanite that could be vitrified. The observed fractionation trend and the granular shapes of akimotoite suggest crystallization from liquid produced by shock melting of the host-rock pyroxene, and the pyroxene glass matrix was probably quenched from the residual melt. However, this interpretation is inconsistent with the static experiments that expect crystallization of majorite ($(Mg,Fe)SiO_3$-garnet), instead of akimotoite, from pyroxene liquid (Sawamoto, 1987). Our discovery raises

the issue on formation mechanisms of the high pressure polymorphs of pyroxene and places additional constraints on the post-shock high-pressure and -temperature conditions of asteroids.

Keywords: Akimotoite, Pyroxene glass, High pressure polymorphs, Meteorite, Shock, Impact

Introduction

Orthopyroxenes [$(Mg,Fe)_2SiO_6$] are among the most important components of stony meteorites and the upper mantle of the Earth. At high-pressure and -temperature conditions, pyroxene transforms to high-pressure polymorphs including majorite ($(Mg,Fe)SiO_3$-garnet), akimotoite ($(Mg,Fe)SiO_3$-ilmenite) and bridgmanite ($(Mg,Fe)SiO_3$-perovskite) (Tschauner el al, 2014), which are considered to be among the major constituents of the Earth's deep mantle (e.g., Liu, 1976; Ohtani et al., 1991; Presnall, 1995). Natural occurrences of these high pressure phases have been mostly discovered in and around shock-induced melt veins of chondrites (Chen et al., 1996; Miyaharaa et al., 2011; Tschauner et al, 2014; Sharp et al., 1997; Tomioka and Fujino, 1997). They provide insight into equilibrium pressure–temperature conditions and the time scale of the dynamic events, and may mimic the phase transformations occurring in the deep Earth mantle and subducted lithosphere (Kerschhofer et al., 1998; Liu et al., 1998; Mosenfelder et al., 2001).

The formation of high-pressure polymorphs of pyroxene in the shock-induced melt veins occurs in various settings and probably involves different mechanisms. The fine-grained crystals in the matrix of the shock melt veins usually result from the crystallization from chondritic melts under high-pressure and high-temperature conditions (Chen et al., 1996; Sharp et al., 1997; Xie et al., 2006b). Large fragments, which were entrained from host rock into the melts, have been generally considered as being in solid-state transformed into polycrystalline assemblages (Ohtani et al., 2004; Tomioka and Fujino, 1997; Xie and Sharp, 2007). In the latter case, the chemical compositions of the high-pressure polymorphs are almost identical to those of the parental pyroxenes in host rock.

In recent years, chemically fractionated ringwoodite-wadsleyite assemblages have been discovered from several highly equilibrated L chondrites. These assemblages were considered to form by fractional crystallization of olivine liquid under high pressure (El Goresy, 2006; Miyahara et al., 2009; Miyahara et al., 2008a). These discoveries address issues on formation processes of high-pressure minerals in heavily shocked meteorites. Is the crystallization of high-pressure polymorphs from mono-mineral melts a unique mechanism for olivine, or a common pheno

mena which also occurs in other mineral systems? On the other hand, the high-pressure polymorphs that were quenched from silicate melts provide natural samples to study melting relations of silicate systems under high-pressure and –temperature conditions, which is important for understanding the early differentiation processes of the Earth and other terrestrial planets (e.g., Hayashi et al., 1979; Kaula,

1979).

In this study, we investigated the shock-induced melt veins in the highly equilibrated ordinary chondrite Grove Mountains (GRV) 052082 (L6). Chemically fractionated olivine-ringwoodite and akimotoite-pyroxene glass assemblages (referred to as Aki- Px Glass assemblages) have been encountered. Here we report the textures and compositional features of the Aki-Px Glass assemblages, and discuss their formation mechanisms. Preliminary results were reported by Feng et al (2011a).

Sample and experiments

A polished thin section was prepared from GRV 052082, a 20.4g stone partly covered with fusion crust and recovered from Grove Mountains in Antarctica by the 22nd Chinese Antarctic Research Expedition. GRV 05082 has been classified as a highly equilibrated low iron ordinary chondritic meteorite (L6), with very homogeneous compositions of olivine ($Fa_{24.1}$) and low-Ca pyroxene ($Fs_{20.7}$) in the host rock (Connolly et al., 2008). It was heavily shocked, with a shock grade of S4 (Connolly et al., 2008). The sample was firstly investigated and documented with an optical microscope, and a scanning electron microscope (SEM) LEO 1450VP equipped with a back-scattered electron (BSE) detector and an energy dispersive spectrometer (EDS). The high-pressure polymorphs in the shock-induced veins were identified by Laser-Raman spectroscopy Renishaw RM-2000 at the Institute of Geology and Geophysics, Chinese Academy of Sciences, and also a JASCO NRS-2000 at the Institute of Mineralogy, Petrology, and Economic Geology, Tohoku

University. Both of the Raman spectrometers used Ar ion lasers producing 514.5 nm lines as the excitation sources. The laser with power of 20-40 mW was focused to ~1-2 μm on the sample and the acquisition time was 30-90s.

The chemical compositions of silicate minerals were determined by the wave-length dispersive technique by JXA 8100 electron microprobe (EPMA) at the Institute of Geology and Geophysics, Chinese Academy of Sciences. The analyses were operated at 15 kV accelerating voltage and 20 nA beam current. The electron beam was focused to about 1 μm in diameter. Diopside (Ca and Si), jadeite (Na), almandine garnet (Fe and Al), orthoclase (K), rhodonite (Mn), forsterite (Mg), synthetic escolaite (Cr), and rutile (Ti) were used as EPMA standards. The standard ZAF matrix correction program was applied to conduct matrix corrections and obtain the chemical compositions. The detection limits are (1 SD): 0.01 wt% for K_2O, Na_2O, and MgO, 0.02 wt% for SiO_2, Cr_2O_3, Al_2O_3 and CaO, 0.03 wt% for TiO_2, FeO and MnO.

The distribution and textures of high-pressure mineral assemblages in the shock-induced veins were then carefully determined and documented by a field emission gun scanning electron microscope (FEG-SEM) JEOL JSM-71010 at an accelerating voltage of 15 kV. An ultra-thin TEM foil from selected target area was surgically cut by Focused Ion Beam system (FIB) JEOL JEM-9320, and extracted by a micromanipulator installed on an optical microscope. The detailed procedure was described by Miyahara et al (2008b). A transmission electron microscope (TEM) JEOL JEM-2010 operating at 200 kV was used for conventional TEM observation

and selected area electron diffraction (SAED). We also used a scanning TEM (STEM), JEOL JEM-3000F field emission TEM operating at 300 kV with a JEOL energy dispersive spectrometer (EDS) detector system, for elemental mapping and quantitative analysis. The chemical compositions of individual grains were obtained by EDS under scanning mode at the STEM. The compositions were corrected with Cliff-Lorimer method (Cliff and Lorimer, 1975) using experimentally determined κ-factors (San Carlos olivine). The detection limits are about 0.1 wt% for main elements. The FEG-SEM, FIB, TEM and STEM analyses were carried out at the Institute of Mineralogy, Petrology, and Economic Geology, Tohoku University in Sendai in Japan.

Results

Silicates in the host rock of GRV 052082 are homogeneous in chemical compositions. The major mineral constituents include olivine ($Fa_{23.2-24.4}$), low-Ca pyroxene ($Fs_{20.5-21.3}$), albitic plagioclase, troilite and metallic Fe-Ni. The EPMA analyses of pyroxene grains in the host rock are listed in Table 1. Shock-induced melt veins are encountered as a network with width up to 2 mm cross cutting the whole thin section (Fig. 1).

Figure 1. Polished thin section of GRV 052082 under transmitted light.

The shock-induced melt veins consist of fine-grained matrix and coarse-grained

silicate fragments. The fine-grained matrix mainly consists of granular or dendritic majorite-pyrope solid solution with grain-size of 1-3 μm, whose interstices are filled with metallic Fe-Ni and troilite blebs (Fig. 2a). Feldspathic clasts depict smooth surfaces on BSE images (Fig. 2a), with some of them converted to maskelynite, and others to lingunite and minor jadeite as identified by Raman spectra (Fig. 3d, e). Original olivine fragments entrained in the shock-melt veins have been transformed into olivine-ringwoodite assemblages, depicting dendrite-like olivine cores (dark) which are depleted in FeO and surrounded by FeO-rich ringwoodite rims (light grey) (Fig. 2b). No wadsleyite was observed in these ringwoodite-olivine assemblages. The textures and chemical fractionation of these ringwoodite-olivine assemblages are also similar to those observed in the heavily shocked GRV 052049 (Feng et al., 2011b), but different from coarse-grained ringwoodite aggregates discovered in other shocked meteorites in previous studies (e.g., Putnis and Price, 1979). Detailed investigation is needed to clarify the formation mechanism of these highly fractionated ringwoodite-olivine assemblages.

Original pyroxene mineral fragments and those in chondrule fragments entrained in the shock-melt veins have been replaced by assemblages of akimotoite crystals and glassy materials (Fig. 2a). High-magnification BSE images reveal a heterogeneous distribution of submicron-sized dark areas among light grey amorphous regions, but more abundant along the rims of the fragments (Fig. 2b and 2d). The boundaries of these clasts are recognizable, although they are blurred by the fine-grained akimotoite in contact with the matrix. It is also noticed that Fe-Ni metal spots disperse within

both the dark fine-grained areas and the grey glass regions. These metal spots are elongated, and orientated within the dark areas (Fig. 2d).

Figure 2. BSE images of pyroxene clasts in the shock-induced vein from GRV 052082.

The Raman spectra of the grey matrix of these pyroxene clasts generally display two broad bands at ~680 and 990 cm^{-1}, which are typical for $MgO\text{-}SiO_2$ glasses (Chen et al., 2004b). However, the Raman spectra obtained from the fine-grained dark areas contain a sharp peak of 804 cm^{-1} (Fig. 3a), the characteristic band of akimotoite. There are few remnant clasts in the enstatite structure (Fig. 3b), or are transformed into poorly-crystallized majorite, as the Raman spectrum shows a low signal/noise ratio (Fig. 3c).

Figure 3. Raman spectra of mineral phases from pyroxene clasts in GRV 052082.

The variation of brightness between pyroxene glass and akimotoite reflects mainly compositional differences. Based on microprobe analyses (Table 1), both phases have low-Ca pyroxene compositions. It is demonstrated that the akimotoite regions are FeO-depleted ($Fs_{14.0\text{-}16.6}$) whereas the pyroxene glassy areas are FeO-enriched ($Fs_{19.6\text{-}23.0}$). By measuring the dark and light grey areas in the Aki-Px Glass assemblage in Fig. 2a, the volume fractions of akimotoite and pyroxene glass are

estimated ~62 vol% and 38 vol%, respectively.

Table 1. Compositions of akimotoite region and pyroxene glass by EPMA.

A FIB-TEM slice was made from the Aki-Px Glass assemblage outlined in Fig. 2a. The bright-field images show granular akimotoite crystals, with sizes ranging from tens to four hundred nanometers (Fig 4). Selected-area electron diffraction revealed different orientations of these akimotoite grains, suggestive of random presence in the pyroxene glass. Furthermore, the akimotoite grains clearly distinguish from pyroxene glass matrix in the Mg and Fe elemental mapping images (Fig. 5). No gradual zoning of the major components were observed along the grain boundaries, indicative of no diffusion. The compositional gap between akimotoite grains (Fs_{6-19}) and pyroxene glass (Fs_{31-39}) is confirmed by STEM-EDS measurements (Table 2). The Fs-contents of akimotoite grains obtained by STEM-EDS are comparable with the microprobe analyses, but with a significantly wider range (Fs_{6-19}) compared with the latter ($Fs_{14.0-16.6}$), which could be due to much smaller excited volumes of the heterogeneous grains by the STEM probe. We also noticed that the Fs-contents of the pyroxene glass obtained by STEM-EDS are significantly higher than those by EPMA, probably due to overlapping tiny akimotoite grains by EPMA.

Figure 4. TEM images of FIB slice.

Figure 5. A BF-STEM image and Si, Mg, Fe, Al and Ca maps of Aki-Px Glass assemblage.

Table 2. Compositions of akimotoite grains and pyroxene glass.

Discussion

Shock-induced P-T conditions of the melt veins

The P-T condition during the shock event can be constrained by the petrographic textures and high pressure mineral inventory in the shock-induced veins of GRV 052082, which are similar to those reported in other heavily shocked ordinary chondrites, *e.g.* Sixiangkou, Tenham, and Yamaoto 791384 (Chen et al., 1996; Miyahara et al., 2010; Price et al., 1979). Based on the results of high-pressure melting experiments of Allende meteorite and KLB-1 peridotite (Agee et al., 1995), the coexistence of ringwoodite, majorite and majorite-pyrope solid solution indicates the pressure of 18-23 GPa and temperature of 2000-2300 °C, similar to other heavily shocked L6 chondrites. However, if the pyroxene glass was vitrified bridgmanite as suggested in previous reports (Chen et al., 2004b; Tomioka and Fujino, 1997), the peak pressure in the shock veins would have exceed 23 GPa.

Formation of chemically fractionated Akimotoite

This is the first discovery of significant chemical fractionation of akimotoite in

silicate fragments relative to the precursor low-Ca pyroxene, which was probably formed via a new mechanism instead of solid-state transformation. Natural akimotoite grains have been reported in and/or adjacent to shock-induced melt veins of heavily shocked chondrites. They occur as: (1) fine-grained euhedral crystals embedded in the matrix of shock-induced melt veins, which were generally enriched in CaO, Al_2O_3 and Na_2O because of melted plagioclase. The akimotoite grains have much lower fe# values (atomic ratio of Fe/Fe+Mg) (0.055) than the host rock low-Ca pyroxene (0.22), and they were considered to have crystallized from chondritic melts (Sharp et al., 1997); (2) polycrystalline aggregates in and/or adjacent to the melt veins, which have nearly the same fe# values of low-Ca pyroxene in the host rocks (e.g. 0.21-0.27 vs 0.22, Ferroir et al., 2008; 0.21 vs 0.22, Tomioka and Fujino, 1997). It suggests no significant diffusion of Fe and/or Mg during the phase transformation. These polycrystalline grains of akimotoite have been so far regarded as isochemical grain boundary or intracrystalline growth of akimotoite at the expense of parental enstatites at subsolidus conditions (Ferroir et al., 2008; Miyahara et al., 2010; Ozawa et al., 2010; Ozawa et al., 2009; Tomioka and Fujino, 1997, 1999; Zhang et al., 2006).

The Aki-Px Glass assemblages in GRV 052082 show a similar occurrence as the polycrystalline grains in shock-melt veins of other meteorites, but these akimotoite crystals in GRV 052082 have significantly different chemical compositions from the host pyroxene (Fig. 6). Compared with the homogeneous pyroxene grains in the host rock (FeO: 13.5 ± 0.3 wt%; MgO: 28.6 ± 0.4 wt%), the akimotoite grains are highly heterogeneous in compositions: depleted in FeO (4.2 - 11.5 wt%) and enriched in

MgO (29.4 - 35.0 wt%). In contrast, the pyroxene glass became relatively FeO-rich (18.8 - 25.6 wt%) and MgO-poor (21.2 - 24.7 wt%). The compositional gaps among the three phases are obvious, and they cannot be explained by solid-state transformation as proposed in previous studies. Alternatively, the observed compositional fractionation between akimotoite and pyroxene glass (Fig. 6) is difficult to be explained by Fe-Mg partition between akimotoite and preexisting bridgmanite at various temperatures. Although the MgO-enrichment of akimotoite relative to bridgmanite is consistent with the phase diagram by Mao et al. (1982), Ito and Yamada (1982) reported different results. Furthermore, the solid-state diffusion of Fe-Mg between akimotoite and preexisting bridgmanite would have produced a wide compositional range in the pyroxene glass (vitrified preexisting bridgemanite), which is comparable to that of the akimotoite grains.

On the other hand, the heterogeneous and FeO-depleted compositions of akimotoite are readily explained by fractional crystallization of akimotoite from melts. With the partition coefficient of FeO between akimotoite and pyroxene melts (0.20-0.44, see the subsection of Partition Coefficient), the FeO-poor and heterogeneous compositions of akimotoite can be modeled by fractional crystallization from a melt that has the composition of low-Ca pyroxene in the host rock (Fig. 7, see the subsection of Partition Coefficient).

The morphology of akimotoite in GRV 052082 supplies additional evidence for its formation, which also suggests crystallization from melt instead of solid-state transformation that usually leads to production of orientated lamellae in the host

mineral (Beck et al., 2005; Chen et al., 2004a). The random distribution of akimotoite grains and the rounded morphology of the clumped grains, confirmed by the selected-area electron diffraction, are consistent with the homogeneous nucleation mechanism during crystallization of a silicate melt (Sharp et al., 1997). The elongated Fe-Ni metal grains in the Aki-Px Glass assemblage (Fig. 2d) are consistent with being molten due to the high temperature. Orientation of the akimotoite and Fe-Ni metal crystals suggests plastic deformation by local stress.

Figure 6. FeO- and MgO- contents of akimotoite, pyroxene in host rock, and pyroxene glass.

The outlines of the Aki-Px Glass assemblages can be clearly recognized in the melt vein matrix. Different from the akimotoite and bridgmanite both crystallized from chondritic melts (Sharp et al., 1997; Xie and Sharp, 2004; Xie et al., 2006b), the whole Aki-Px Glass assemblages show a stoichiometric composition of low-Ca pyroxene and no coexisting ringwoodite was discovered. According to the EPMA results, the concentrations of minor elements Al and Ca in these assemblages are also close to those of low-Ca pyroxene in the host rock (Table 1). The presence of minor Na_2O in the akimotoite grains (Table 1) is consistent with crystallization from Na-bearing melts, and Na was likely diffused from the surrounding chondritic melt. Therefore, the Aki-Px Glass assemblages are considered to originate from preexisting low-Ca pyroxene grains which were little contaminated by the surrounding materials.

Based on the petrographic and compositional features, we propose that the akimotoite in these assemblages were formed by fractional crystallization of nearly pure pyroxene melts, which were produced via melting preexisting low-Ca pyroxene clasts by the shock event. However, we have also noticed that the phase diagram based on static high pressure experiments of pyroxene expects majorite, instead of akimotoite, to crystallize directly from the pyroxene liquid (Sawamoto, 1987). This discrepancy raises the issue of formation mechanisms of high pressure polymorphs of pyroxene.

Origin of Px Glass and crystallization process of Aki-Px Glass assemblages

Another key issue related with formation process of the Aki-Px Glass assemblages is the origin of the pyroxene glass. (Mg, Fe)SiO_3-glass has been frequently discovered in melt veins of many chondrites, coexisting with high pressure polymorphs of pyroxene, i.e. majorite and/or akimotoite (Chen et al., 2004b; Ferroir et al., 2008; Miyahara et al., 2010). The (Mg, Fe)SiO_3-glass in these petrographic settings has nearly identical chemical compositions of low-Ca pyroxene in the host meteorites, and it was considered to be vitrified bridgmanite that formed by solid-state transformation at high pressures >23 GPa. The amorphization of bridgmanite is likely due to irradiation of laser or electron beam during measurement of this phase, as suggested by recent discovery of bridgmanite in similar assemblages (Tschauner et al., 2014). The bridgmanite grains have nearly identical compositions of the coexisting

akimotoite, and both are similar to that of the low-Ca pyroxene in the host rock (Tschauner et al., 2014). The latter study confirms the solid-state transformation of bridgmanite. Although the Aki-Px Glass assemblages in GRV 052082 show a texture similar to that of coexisting akimotoite and bridgmanite (or vitrified bridgmanite) reported in other meteorites, the akimotoite and pyroxene glass in the Aki-Px Glass assemblages are highly fractionated in compositions, different from the previous results mentioned above. Therefore, these Aki-Px Glass assemblages in GRV 052082 should not have been formed by the same mechanism of solid-state transformation.

Alternatively, the pyroxene glass in the Aki-Px Glass assemblages could be vitrified bridgmanite that crystallized from silicate melts. Amorphous $(Mg,Fe)SiO_3$-grains coexisting with akimotoite and ringwoodite were reported in shock-induced melt vein matrix, and they were considered as vitrified bridgmanite crystallized from melts (Sharp et al., 1997). The amorphous $(Mg,Fe)SiO_3$-grains are idiomorphic, surrounded by crystals of akimotoite and/or ringwoodite (Sharp et al., 1997; Xie et al., 2006b). This is obviously different from the granular grains of akimotoite embedded in the pyroxene glass matrix in GRV 052082 (Figs. 2 and 4), arguing for their distinct forming mechanisms. Furthermore, experimentally determined high-pressure and -temperature phase diagrams also forsee bridgmanite crystallization prior to akimotoite during pressure release (e.g., Hirose et al., 2001). Hence, the phase diagrams argue against the possibility that the pyroxene glass was vitrified from preexisting bridgmanite. Furthermore, FeO is significantly enriched in the pyroxene glass (18.8-25.6 wt%) compared with the pyroxene in the host rock

(13.5±0.3 wt%). According to the analyses of bridgmanite in fine-grained melt veins in shocked chondrites (Sharp et al., 1997; Xie et al., 2006b) and that recovered from the high-pressure and -temperature experiments (Asahara et al., 2004; Corgne et al., 2005; Hirose et al., 2004; Liebske et al., 2005; McFarlane et al., 1994; Tange et al., 2009; Trønnes and Frost, 2002), the partition coefficients of FeO between bridgmanite and chondritic/silicate melts are less than 1. Hence, bridgmanite first crystallized from the chondritic/silicate melts would be FeO-depleted, different from the significant FeO-enrichment of the pyroxene glass.

Another formation scenario of the pyroxene glass is that it was quenched from the residual melts after fractional crystallization of FeO-depleted akimotoite, which had become FeO-enriched as precipitating of the latter. This scenario is consistent with all observations, including the occurrence of the granular akimotoite crystals in the pyroxene glass, the FeO-depletion of the akimotoite and the FeO-enrichment of the pyroxene glass. These Aki-Px Glass assemblages can be elucidated as following：The original pyroxene fragments were selectively molten during the peak shock pulse (18-23 GPa) around 2300 ^{o}C, because it contains 20 mol% of $FeSiO_3$ that lowers its melting temperature comparing with pure $MgSiO_3$-pyroxene (Fei and Bertka, 1999; Huebner and Turnock, 1980; Presnall, 1995). Akimotoite with low FeO-contents crystallized from the pyroxene melts as the temperature decreased rapidly to the akimotoite stability field, i.e. lower than 2000 ^{o}C at ~20 GPa (Gasparik, 1990; Presnall et al., 1995; Wentzcovitch et al., 2004). With crystallization of FeO-poor akimotoite, the residual melt became enriched in FeO, which finally was quenched to

glass. The heterogeneity of pyroxene glass in the same assemblages suggests that the quenching was very fast due to heat waste.

Normally, shock-induced melt veins and pockets in meteorites are fine-grained mixtures of melted regions and have compositions close to the bulk meteorites. As discussed above, the Aki-Px Glass assemblages likely crystallized from nearly pure pyroxene melts. The presence of pyroxene melts was probably due to large sizes of the precursor pyroxene fragments, which could help the melts to preserve their original compositions without mixing surrounding material. In addition, crystallization of akimotoite first along the boundaries of the pyroxene melts formed "wall" of the assemblages, further protecting from mixing the surrounding material. Similar features have been observed in ringwoodite-olivine assemblages in the shocked Grove Mountains ordinary chondrites (Feng et al., 2007 and 2011) and in the ringwoodite-wadsleyite assemblages reported by Miyahara et al. (2009). In these assemblages, ringwoodite was proposed to crystallize from pure olivine melts.

Partition coefficient of FeO between Akimotoite and Pyroxene melt

According to the formation process outlined above, the chemical compositions of akimotoite grains are constrained by the FeO partition coefficient between akimotoite and pyroxene melt. Because no melting experiment of akimotoite has been conducted so far, the partition coefficient of divalent cations between akimotoite and pyroxene melt need to be experimentally determined. However, the small and euhedral grains of akimotoite in shock-induced melt veins were previously proposed to crystallize from

melts with chondritic compositions (Sharp et al., 1997; Xie and Sharp, 2004). We tested the possibility of obtaining the partition coefficient of the divalent cations into akimotoite using the obtained data of the bulk composition of an L- chondritic melt (Chen et al., 1996) and the chemical compositions of akimotoite embedded in the melt vein matrix (Sharp et al., 1997; Xie and Sharp, 2004). We calculated the partition coefficients (K) of FeO between akimotoite and chondritic melt as: $K^{Aki\text{-}melt} = M^{Aki} / M^{melt}$, where M is FeO wt%. The obtained $K^{Aki\text{-}Melt}$ is in the range of 0.20 - 0.44.

According to the fractional crystallization process of akimotoite from pyroxene melt in GRV 052082, we calculated the partition coefficient of FeO between akimotoite and pyroxene melt with the following two methods. Assuming that akimotoite of lowest Fs value was crystallized first from the pyroxene melt, K_1 can be defined as: $K_1 = M^{Aki\ of\ lowest\ Fs\ value}/M^{pyroxene\ in\ host\ rock}$. In the second method, the akimotoite and the pyroxene glass of highest Fs value can be considered to have formed at the end of crystallization sequence, therefore we calculated K_2 by: $K_2 = M^{Aki\ of\ highest\ Fs\ value} / M^{px\ glass\ of\ highest\ Fs\ value}$. As a result, K_1 is 0.31; K_2 is 0.44, respectively. Both of them are in the same range as that of akimotoite in melt vein matrix of L chondrites.

Based on the Rayleigh Law, the ratio of element concentration in the residual melt over the initial concentration in the melt can be expressed as:

$$C_L = C_0 F^{(k-1)} \qquad (i)$$

where C_L = concentration of the element in the residual melt, C_0 = initial concentration of the element in the melt, F = fraction of the melt that remains, and K

= bulk partition coefficient for the crystallizing solids. Using the determined K_1 and K_2 values of FeO, with the chemical composition of pyroxene in host rock, we can model the compositional path of akimotoite crystallizing from pyroxene melt under high pressure and –temperature conditions in GRV 052082. The curves of FeO contents in akimotoite and residue melt are shown in Figure 7. It is noticed that the measured values for akimotoite are consistent with the predicted trend while values obtained for the pyroxene glass are close to that of the residual melt. The upper limits of FeO in both akimotoite and pyroxene glass intersect the K_2 curves at the same points (black arrows on Fig. 7), which represents that based on K_2, the FeO-enriched akimotoite and pyroxene glass formed at the same stage of akimotoite crystallization when ~30% melt was left as residual. The residual melt was probably quenched fast, without more FeO-enriched akimotoite crystallized. Although we ignored the temperature and pressure variation during the crystallization, the simplified modeling results are basically consistent with our observations. The predicted abundances of akimotoite (~70%) and pyroxene glass (~30%) are also close to the measurements, 62 vol% akimotoite and 38 vol% pyroxene glass.

Figure 7: Variation of FeO concentrations during fractional crystallization of akimotoite from the pyroxene melt

Melting of silicates and crystallization of high-pressure minerals

Fractional crystallization of ringwoodite-wadsleyite assemblages from olivine

melt has been reported in heavily shocked L6-chondrites (Miyahara et al., 2009; Miyahara et al., 2008a). Our study also shows that melting of a single silicate mineral and subsequent fractional crystallization of high-pressure polymorphs are not restricted to olivine-material minerals, but also take place in other constitutes of chondrites. Melting of enstatite under high pressures (~2400 ^{o}C at 18 GPa) (Ohtani and Kumazawa, 1981; Presnall and Gasparik, 1990) slightly exceeds the estimated shock-induced temperature of the melt vein (18-23 GPa, 2000-2300 ^{o}C). But with the increase of FeO content, the melting temperature of pyroxene decreases (Huebner and Turnock, 1980), which could lead to the formation of (Mg, Fe)SiO_3-melt from parental low-Ca pyroxene grains enclosed in the shock-induced melt veins.

Akimotoite has been considered as a high-pressure, low-temperature mineral, since it is stable under pressures of >20 GPa and temperatures of <1800 °C (Fei and Bertka, 1999; Sawamoto, 1987). It was determined as a subsolidus phase and is not predicted to crystallize from chondritic or mono-pyroxene melts based on high pressure experiments (Sawamoto, 1987; Agee et al., 1995; Gasparik, 1992; Zhang and Herzberg, 1994). Therefore, it was suggested that akimotoite discovered in the matrix of shock-induced melt veins crystallized metastably from a supercooled melt during fast quenching (Sharp et al., 1997; Xie and Sharp, 2004; Xie et al., 2006a; Xie et al., 2006b), which is supportive of our model. Crystallization and preservation of akimotoite indicates that the temperature decreased fast; in the meantime, the duration of high pressure (~20 GPa) in the shock event on asteroid parent body was long enough (Beck et al., 2005) to allow the growth of high pressure minerals up to

hundreds of nanometers. Another scenario is that akimotoite might be in solid-state transformed from preexisting majorite that first crystallized from the pyroxene melt.

Implications

Chemically fractionated akimotoite-pyroxene glass assemblages were discovered in shock-induced melt veins in the L6 chondrite GRV 052082, associated with ringwoodite-olivine assemblages that suggested a pressure of 18-23 GPa and a temperature of 2000-2300 ^{o}C produced by a shock event. Detailed study of these assemblages suggest that the akimotoite grains crystallized from mono-pyroxene melt and the pyroxene glass was quenched from the residual melt. However, crystallization of akimotoite directly from liquid is inconsistent with the phase diagram of pyroxene (Sawamoto, 1987). This discrepancy may be explained by crystallization of supercooled melts or solid-state transformation of preexisting majorite.

This work suggests a new mechanism for the formation of akimotoite besides the solid-state transformation and crystallization from chondritic melts reported in previous studies. The significantly fractionated akimotoite-pyroxene glass assemblages provide with natural samples for elemental partition between akimotoite and pyroxene glass, and the results will shed light on the high-pressure experiments of the Earth's and planetary mantle. Furthermore, the significant chemical fractionation between akimotoite and residual melt will constrain the P-T-t track during asteroid impact events, if the partition and diffusion coefficients will be determined.

Acknowledgements:

The meteorite sample was supplied by the Polar Research Institute of China. Our study was supported by the Natural Science Foundation of China (41430105, 41273077，41203048, 41521062). L. Feng was also financially supported by Tohoku University Global COE program "Global Education and Research Center for Earth and Planetary Dynamics" and the Max-Planck Society Foundation. We would like to thank M. Kimura and other four anonymous reviewers and the Associate Editors Dr. Sergio Speziale and Dr. Liu for their useful comments that led to significant improvement of this paper.

Reference

Agee C. B., Li J., Shannon M. C., and Circone S. (1995) Pressure -Temperature phase-diagram for the Allende Meteorite. *Journal of Geophysical Research-Solid Earth* **100**, 17725-17740.

Asahara Y., Kubo T., and Kondo T. (2004) Phase relations of a carbonaceous chondrite at lower mantle conditions. *Physics of the Earth and Planetary Interiors* **143-144**, 421-432.

Beck P., Gillet Ph., El Goresy A., and Mostefaoui S. (2005) Timescales of shock processes in chondritic and martian meteorites. *Nature* **435**, 1071-1074.

Chen M., El Goresy A., and Gillet Ph. (2004a) Ringwoodite lamellae in olivine: Clues to olivine-ringwoodite phase transition mechanisms in shocked meteorites and in subducting slabs. *Proceedings of the National Academy of Sciences of the*

United States of America **101**, 15033-15037.

Chen M., Sharp T. G., El Goresy A., Wopenka B., and Xie X. (1996) The Majorite-Pyrope + Magnesiowustite Assemblage: Constraints on the History of Shock Veins in Chondrites. *Science* **271**, 1570-1573.

Chen M., Xie X., and El Goresy A. (2004b) A shock-produced (Mg, Fe)SiO_3 glass in the Suizhou meteorite. *Meteoritics & Planetary Science* **39**, 1797-1808.

Cliff, G., and Lorimer, G.W. (1975) The quantitative analysis of thin specimens. *Journal of Microscopy*, **103**, 203-207.

Connolly, H.C., Smith, C., Benedix, G., Folco, L., Righter, K., Zipfel, J., Yamaguchi, A., and Aoudjehane, H.C. (2008) The Meteoritical Bulletin, No. 93, 2008 March. *Meteoritics & Planetary Science*, **43**, 571-632.

Corgne A., Liebske C., Wood B. J., Rubie D. C., and Frost D. J. (2005) Silicate perovskite-melt partitioning of trace elements and geochemical signature of a deep perovskitic reservoir *Geochemica et Cosmochimica Acta* **69**, 485-496.

El Goresy A. (2006) Olivine to ringwoodite and wadsleyte phase transformation mechanisms in naturally shocked chondritic meteorites: Clues to incoherent, coherent growths and retrograde transitions. *AGU Fall Meeting Abstracts* **54**, 08.

Fei Y. and Bertka C. M. (1999) Phase transitions in the Earth's mantle and mantle mineralogy. In *Mantle Petrology: Field Observations and High-Pressure Experimentation: A Tribute to F. R. Boyd* (ed. C. M. B. Y. Fei, and B. O. Mysen), pp. 189-207. Geochemical Society.

Feng, L., Lin, Y., Hu, S., Xu, L., and Miao, B. (2007) Assemblages of Olivine Polymorphs in Grove Mountains (GRV) 052049: Constraints on Pressure-Temperature Condition of Shock Metamorphism (abstract). *Meteoritics & Planetary Science*, **42**, A45.

Feng L., Miyahara M., Nagase T., Ohtani E., Hu S., El Goresy A., and Lin Y. (2011a) Shock Conditions and Formation Mechanism of Akimotoite-Pyroxene Glass Assemblages in the Grove Mountains (GRV) 052082. In *Japan Geooscience Union Meeting*, Chiba, Japan.

Feng, L., Lin, Y., Hu, S., Xu, L., and Miao, B. (2011b) Estimating compositions of natural ringwoodite in the heavily shocked Grove Mountains 052049 meteorite from Raman spectra. *American Mineralogist*, **96**, 1480-1489.

Ferroir T., Beck P., Moortèle B. V. d., Bohn M., Reynard B., Simionovici A., El Goresy A., and Gillet Ph. (2008) Akimotoite in the Tenham meteorite: Crystal chemistry and high-pressure transformation mechanisms. *Earth and Planetary Science Letters* **275**, 26-31.

Gasparik T. (1990) Phase relations in the transition zone. *Journal of Geophysical Research* **95**, 15751-715769.

Gasparik T. (1992) Melting experiments on the enstatite-pyrope join at 80-152 Kbar. *Journal of Geophysical Research* **97,** 15181-15188.

Hayashi C., Nakazawa K., and Mizuno H. (1979) Earth's melting due to the blanketing effect of the primordial dense atmosphere. *Earth and Planetary Science Letters* **43**, 22-28.

Hirose K., komabayashi T., Murakami M., and Funakoshi K. (2001) In situ measurements of the majorite-akimotoite-perovskite phase transition boundaries in $MgSiO_3$. *Geophysical Research Letters* **28**, 4351-4354.

Hirose K., Shimizu N., Westrenen W., and Fei Y. (2004) Trace element partitioning in Earth's lower mantle and implications for geochemical consequences of partial melting at the core–mantle boundary *Physics of The Earth and Planetary Interiors* **146**, 249-260.

Huebner J. S. and Turnock A. C. (1980) The melting relations at 1 bar of pyroxenesc omposed largely of Ca-, Mg-, and Fe-bearing components. *American Mineralogist* **65**, 225-271.

Ito, E., and Yamada, H. (1982) Stability relations of silicate spinels, ilmenites, and perovskites. In S. Akimoto, and M.H. Manghnani, Eds. *High-Pressure Research in Geophysics*, **12**, 405-419. Center for Academic Publications, Tokyo.

Kaula W. M. (1979) Thermal evolution of Earth and Moon growing by planetesimal impacts. *Journal of Geophysical Research* **84**, 999–1008.

Kerschhofer L., Dupas C., Liu M., Sharp T. G., Durham W. B., and Rubie D. C. (1998) Polymorphic transformations between olivine, wadsleyite and ringwoodite; mechanisms of intracrystalline nucleation and the role of elastic strain. *Mineralogical Magazine* **62**, 617-638.

Liebske C., Corgne A., Frost D. J., Rubie D. C., and Wood B. J. (2005) Compositional effects on element partitioning between Mg-silicate perovskite

and silicate melts. *Contributions to Mineralogy and Petrology* **149**, 103-128.

Liu L.-G. (1976) The high-pressure phases of $MgSiO_3$ *Earth and Planetary Science Letters* **31**, 200-208.

Liu M., Kerschhofer L., and Monsenfelder J. L. (1998) The effect of strain energy on growth rates during the olivine-spinel transformation and implications for olivine metastability in subducting slabs. *Journal of Geophysical Research* **103**, 23897-23909.

Mao, H.K., Bell, P.M., and Yagi, T. (1982) Iron-magnesium fractionation model for the earth. In S. Akimoto, and M.H. Manghnani, Eds. *High-Pressure Research in Geophysics*, **12**, 319-325. Center for Academic Publications, Tokyo.

McFarlane E. A., Drake M. J., and Rubie D. C. (1994) Element partitioning between Mg-perovskite, magnesiowüstite, and silicate melt at conditions of the Earth's mantle. *Geochemica et Cosmochimica Acta* **58**, 5161-5172.

Miyahara M., El Goresy A., Ohtani E., Kimura M., Ozawa S., Nagase T., and Nishijima M. (2009) Fractional crystallization of olivine melt inclusion in shock-induced chondritic melt vein. *Physics of the Earth and Planetary Interiors* **177**, 116-121.

Miyahara M., El Goresy A., Ohtani E., Nagase T., Nishijima M., Vashaei Z., Ferroir T., Gillet Ph., Dubrovinsky L., and Simionovici A. (2008a) Evidence for fractional crystallization of wadsleyite and ringwoodite from olivine melts in chondrules entrained in shock-melt veins. *Proceedings of the National Academy of Sciences of the United States of America* **105**, 8542-8547.

Miyahara M., Ohtani E., Kimura M., El Goresy A., Ozawa S., Nagase T., Nishijima M., and Hiragae K. (2010) Coherent and subsequent incoherent ringwoodite growth in olivine of shocked L6 chondrites. *Earth and Planetary Science Letters* **295**, 321-327.

Miyahara M., Ohtani E., Ozawa S., Kimura M., El Goresy A., Sakai T., Nagase T., Hiraga K., Hirao N., and Ohishi Y. (2011) Natural dissociation of olivine to (Mg,Fe)SiO_3 perovskite and magnesiowüstite in a shocked Martian meteorite. *Proceedings of the National Academy of Sciences of the United States of America* **108**, 5999-6003.

Miyahara M., Sakai T., Ohtani E., Kobayashi Y., Kamada S., Tadashi Kondo, Nagase T., Yoo J. H., Nishijima M., and Vashaei Z. (2008b) Application of FIB system to ultra-high-pressure Earth science. *Journal Of Mineralogical and Petrological Science* **103**, 88-93.

Mosenfelder J. L., Marton F. C., Ross II C. R., Kerschhofer L., and Rubie D. C. (2001) Experimental constraints on the depth of olivine metastability in subducting lithosphere. *Physics of the Earh and Planetary Interiors* **127**, 165-180.

Ohtani E., Kagawa N., and Fujino K. (1991) Stability of majorite (Mg, Fe)SiO_3 at high pressures and 1800 °C. *Earth and Planetary Science Letters* **102**, 158-166.

Ohtani E., Kimura Y., Kimura M., Takata T., Kondo T., and Kubo T. (2004) Formation of high-pressure minerals in shocked L6 chondrite Yamato 791384: constraints on shock conditions and parent body size. *Earth and Planetary*

Science Letters **227**, 505-515.

Ohtani E. and Kumazawa M. (1981) Melting of forsterite Mg_2SiO_4 up to 15 GPa. *Physics of the Earth and Planetary Interiors* **32**, 32-38.

Ozawa S., Miyahara M., Ohtani E., Kimura M., and Ito Y. (2010) Petrography of Yamato 984028 lherzolitic shergottite and its melt vein: Implications for its shock metamorphism and origin of the vein. *Polar Science*, 550-557.

Ozawa S., Ohtani E., Miyahara M., Suzuk A., Kimura M., and Ito Y. (2009) Transformation textures, mechanisms of formation of high-pressure minerals in shock melt veins of L6 chondrites, and pressure-temperature conditions of the shock events. *Meteoritics & Planetary Science* **44**, 1771-1786.

Presnall D. C. (1995) Phase diagrams of Earth-forming minerals. In *Mineral Physics & Crystallography: A Handbook of Physical Constants* (ed. T. J. Ahrens), pp. 248-268. American Geophysical Union, Washington, D. C.

Presnall D. C. and Gasparik T. (1990) Melting of Enstatite ($MgSiO_3$) from 10 to 16.5 GPa and the Forsterite (Mg_2SiO_4)-Majorite ($MgSiO_3$) Eutectic at 16.5 GPa: Implications for the Origin of the Mantle. *Journal of Geophysical Research* **95**(95), 15771-15777.

Price G. D., Putnis A., and Agrell S. O. (1979) Electron Petrography of Shock-Produced Veins in the Tenham Chondrite. *Contributions to Mineralogy and Petrology* **71**, 211-218.

Putnis A. and Price G. D. (1979) High-pressure $(Mg,Fe)_2SiO_4$ phases in the Tenham chondritic meteorite. *Nature*, 217-218.

Sawamoto H. (1987) Phase Diagram of $MgSiO_3$ at Pressures up to 24 GPa and Temperatures up to 2200 °C: Phase Stability and Properties of Tetragonal Garnet. In *High-Pressure Research in Mineral Physics: A Volume in Honor of Syun-iti Akimoto* (eds. M. H. Manghnani and Y. Syono). American Geophysical Union, Washington, D. C.

Sharp T. G., Lingemann C. M., Dupas C., and Stöffler D. (1997) Natural Occurrence of $MgSiO_3$-Ilmenite and Evidence for $MgSiO_3$-Perovskite in a Shocked L Chondrite. *Science* **277**, 352-355.

Tange Y., Eiichi Takahashi, Nishihara Y., Funakoshi K., and Sata N. (2009) Phase relations in the system MgO-FeO-SiO_2 to 50 GPa and 2000 ^{o}C: An application of experimental techniques using multianvil apparatus with sintered diamond anvils. *Journal of Geophysical Research* **114**, B02214.

Tomioka N. and Fujino K. (1997) Natural (Mg,Fe)SiO3-Ilmenite and -Perovskite in the Tenham Meteorite. *Science* **277**, 1084-1086.

Tomioka N. and Fujino K. (1999) Akimotoite, $(Mg,Fe)SiO_3$, a new silicate mineral of the ilmenite group in the Tenham chondrite. *American Mineralogist* **84**, 267-271.

Trønnes R. G. and Frost D. J. (2002) Peridotite melting and mineral–melt partitioning of major and minor elements at 22–24.5 GPa. *Earth and Planetary Science Letters* **197**, 117-131.

Tschauner O., Ma C., Beckett J. R., Prescher C., Prakapenka V. B., and Rossman G R. (2014) Discovery of bridgmanite, the most abundant mineral in Earth, in a

shocked meteorite. *Science* **346**, 1100-1102.

Wentzcovitch R. M., Stixrude L., Karki B. B., and Kiefer B. (2004) Akimotoite to perovskite phase transition in $MgSiO_3$. *Geophysical Research Letters* **31**, L10611.

Xie Z. and Sharp T. G. (2004) High-pressure phases in shock-induced melt veins of the Umbarger L6 chondrite: Constraints of shock pressure. *Meteoritic and Planetary Science* **39**, 2043-2054.

Xie Z. and Sharp T. G. (2007) Host rock solid-state transformation in a shock-induced melt vein of Tenham L6 chondrite. *Earth and Planetary Science Letters* **254**, 433-445.

Xie Z., Sharp T. G., and DeCarli P. S. (2006a) Estimating shock pressures based on high-pressure minerals in shock-induced melt veins of L chondrites. *Meteoritics & Planetary Science* **12**,1883-1898.

Xie Z., Sharp T. G., and DeCarli P. S. (2006b) High-pressure phases in a shock-induced melt vein of the Tenham L6 chondrite: Constraints on shock pressure and duration. *Geochimica et Cosmochimica Acta* **70**, 504-515.

Zhang A., Hsu W., Wang R., and Ding M. (2006) Pyroxene polymorphs in melt veins of the heavily shocked Sixiangkou L6 chondrite. *European Journal of Mineralogy* **18**, 719-726.

Zhang J. and Herzberg C. (1994) Melting experiments on anhydrous peridotite KLB-1 from 5.0-22.5 GPa. *Journal of Geophysical Research* **99**, 17729-17742.

This is a preprint, the final version is subject to change, of the American Mineralogist (MSA)
Cite as Authors (Year) Title. American Mineralogist, in press.
(DOI will not work until issue is live.) DOI: http://dx.doi.org/10.2138/am-2017-5905

Table 1. Compositions of akimotoite region and pyroxene glass by EPMA, in comparison with pyroxene grains in host rock, in wt%.

	Akimotoite				Pyroxene glass				Pyroxene in host	
									n=8	SD
SiO_2	57.4	57.1	56.7	56.9	56.4	56.0	54.9	55.2	56.1	*0.48*
TiO_2	0.18	0.19	0.19	0.13	0.16	0.17	0.17	0.19	0.18	*0.05*
Al_2O_3	0.15	0.15	0.14	0.17	0.08	0.13	0.14	0.13	0.15	*0.04*
Cr_2O_3	0.11	0.11	0.10	0.45	0.10	0.08	0.04	0.09	0.15	*0.03*
FeO	9.37	10.1	10.8	10.1	12.6	13.7	14.5	13.7	13.49	*0.28*
MnO	0.42	0.54	0.46	0.47	0.61	0.68	0.76	0.74	0.48	*0.04*
MgO	31.9	31.1	30.1	30.9	28.8	26.9	27.0	26.9	28.6	*0.38*
CaO	0.64	0.65	0.83	0.94	0.83	1.00	0.66	0.95	0.90	*0.08*
Na_2O	0.32	0.67	0.78	0.99	1.27	1.67	2.00	1.87	0.03	*0.02*
K_2O	n.d.	0.04	0.01	0.01	0.01	n.d.	0.01	0.02	0.01	*0.01*
Total	100.49	100.65	100.11	101.06	100.86	100.33	100.18	99.79	100.08	*0.75*
					Formula (O = 6)					
Si	1.999	1.989	1.993	1.972	1.978	1.986	1.946	1.964		2.006
Ti	0.005	0.005	0.005	0.003	0.004	0.005	0.005	0.005		0.005
Al	0.006	0.006	0.006	0.007	0.003	0.005	0.006	0.005		0.006
Cr	0.003	0.003	0.003	0.012	0.003	0.002	0.001	0.003		0.004
Fe	0.273	0.294	0.317	0.293	0.370	0.406	0.430	0.408		0.403
Mn	0.012	0.016	0.014	0.014	0.018	0.020	0.023	0.022		0.015
Mg	1.656	1.615	1.577	1.597	1.506	1.422	1.427	1.427		1.524
Ca	0.024	0.024	0.031	0.035	0.031	0.038	0.025	0.036		0.034
Na	0.022	0.045	0.053	0.067	0.086	0.115	0.137	0.129		0.002

This is a preprint, the final version is subject to change, of the American Mineralogist (MSA)
Cite as Authors (Year) Title. American Mineralogist, in press.
(DOI will not work until issue is live.) DOI: http://dx.doi.org/10.2138/am-2017-5905

Table 2. Compositions of akimotoite grains and pyroxene glass obtained by STEM-EDS, normalized to 100%

	Akimotoite				Pyroxene glass			
SiO_2	55.5	55.5	55.3	56.2	50.4	50.7	52.2	51.3
FeO	9.6	7.6	11.5	5.4	18.8	22.6	21.1	19.1
CaO	1.4	0.4	0.5	0.3	4.5	1.1	1.3	1.1
Al_2O_3	3.5	3.5	3.3	3.7	3.2	2.8	3.1	3.0
MgO	30.0	33.0	29.4	34.4	23.1	22.9	22.3	25.5
Total	100	100	100	100	100	100	100	100
				Formula (O = 6)				
Si	1.94	1.92	1.95	1.93	1.87	1.90	1.93	1.89
Fe	0.28	0.22	0.34	0.16	0.58	0.71	0.65	0.59
Ca	0.05	n.d	0.02	n.d	0.18	0.04	0.05	0.04
Al	0.14	0.14	0.14	0.15	0.14	0.12	0.13	0.13
Mg	1.56	1.71	1.54	1.76	1.28	1.28	1.23	1.40
Fs	15	11	18	8	31	36	35	30

Note: The analytical uncertainties were estimated <5% (1SD), based on repeated analyses of a small region of the pyroxene glass

Figure Captions

Figure 1. Polished thin section of GRV 052082 under transmitted light. The shock-induced melt veins are opaque (arrows).

Figure 2. BSE images of pyroxene clasts in the shock-induced vein from GRV 052082. (a) High- pressure mineral assemblages from a chondritic clast. The FIB-TEM slice is shown in the dashed-line frame. White box locates image (b). (b) High magnification image of bright pyroxene glass area ($Fs_{23.2}$) and the dark akimotoite grains ($Fs_{17.3}$). (c) High-pressure mineral assemblages in the shock-induced vein. White box locates image. (d) High magnification image of bright pyroxene glass area ($Fs_{21.4}$) and dark akimotoite crystals ($Fs_{15.5}$). Note the black arrow pointing to the direction of elongation of akimotoite and metal. Abbreviations: Mas = Maskelynite; Hol = Lingunite; Px Glass = Pyroxene Glass; Aki = Akimotoite; Ol = Olivine; Rgt = Ringwoodite; Jad = Jadeite.

Figure 3. Raman spectra of mineral phases from pyroxene clasts and those of lingunite and jadeite in GRV 052082.

Figure 4. (a) Bright-field TEM (BF-TEM) image of FIB slice from Aki-Px Glass assemblage. Idiomorphic crystals of akimotoite (Aki) embedded in amorphous pyroxene glass (Px-Glass). (b) SAED pattern of an akimotoite crystallite along the

zonal axis [$\bar{3}$**00**].

Figure 5. A bright-field (BF)-STEM image and Si, Mg, Fe, Al and Ca maps of Aki-Px Glass assemblage. The arrows in Mg-K_α and Fe-K_α maps point to the akimotoite crystallites. Color bars on the left are intensity of K_α lines of the elements.

Figure 6. Plots of FeO- and MgO- contents of akimotoite, pyroxene in host rock, and pyroxene glass.

Figure 7: Variation of FeO and MgO concentrations in akimotoite (Aki) and pyroxene melt (Px melt) vs. fraction of melt remaining based on equation (*i*). Solid lines are calculated curves of pyroxene melt and dashed lines are of akimotoite. Green and yellow areas are compositional ranges of akimotoite and pyroxene glass detected in GRV 052082.

This is a preprint, the final version is subject to change, of the American Mineralogist (MSA)
Cite as Authors (Year) Title. American Mineralogist, in press.
(DOI will not work until issue is live.) DOI: http://dx.doi.org/10.2138/am-2017-5905

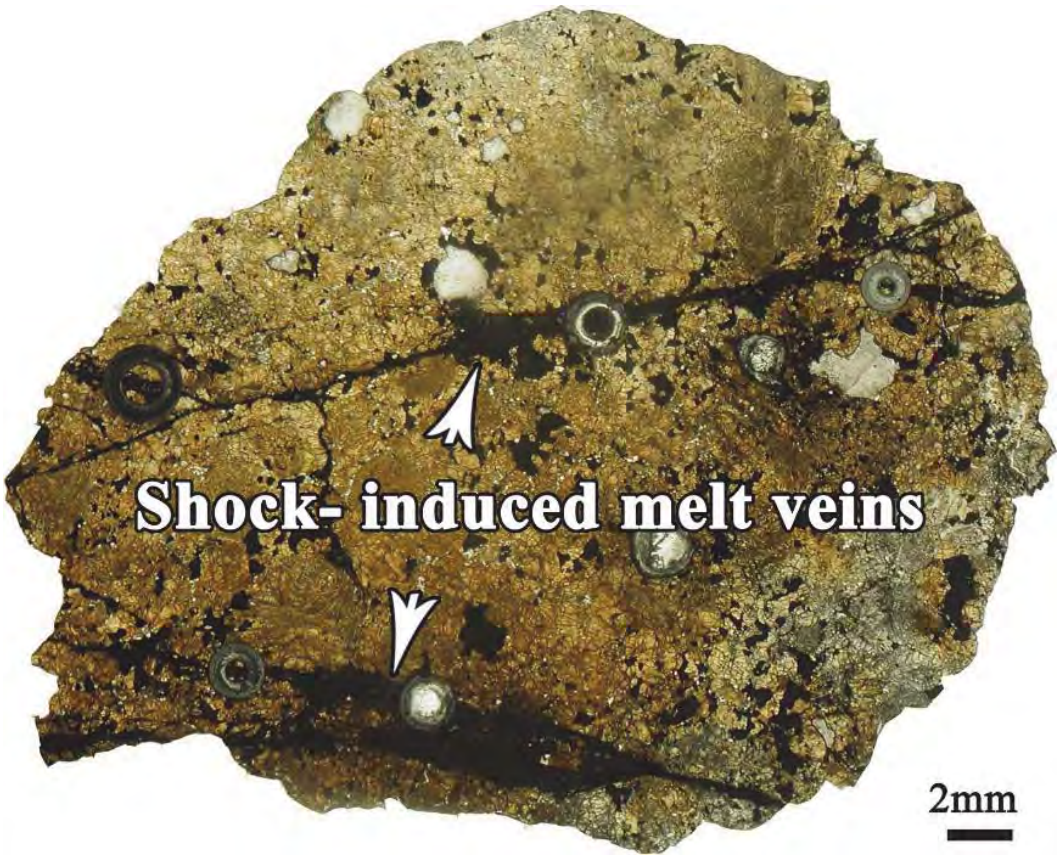

Fig. 1 By Feng et al.

This is a preprint, the final version is subject to change, of the American Mineralogist (MSA)
Cite as Authors (Year) Title. American Mineralogist, in press.
(DOI will not work until issue is live.) DOI: http://dx.doi.org/10.2138/am-2017-5905

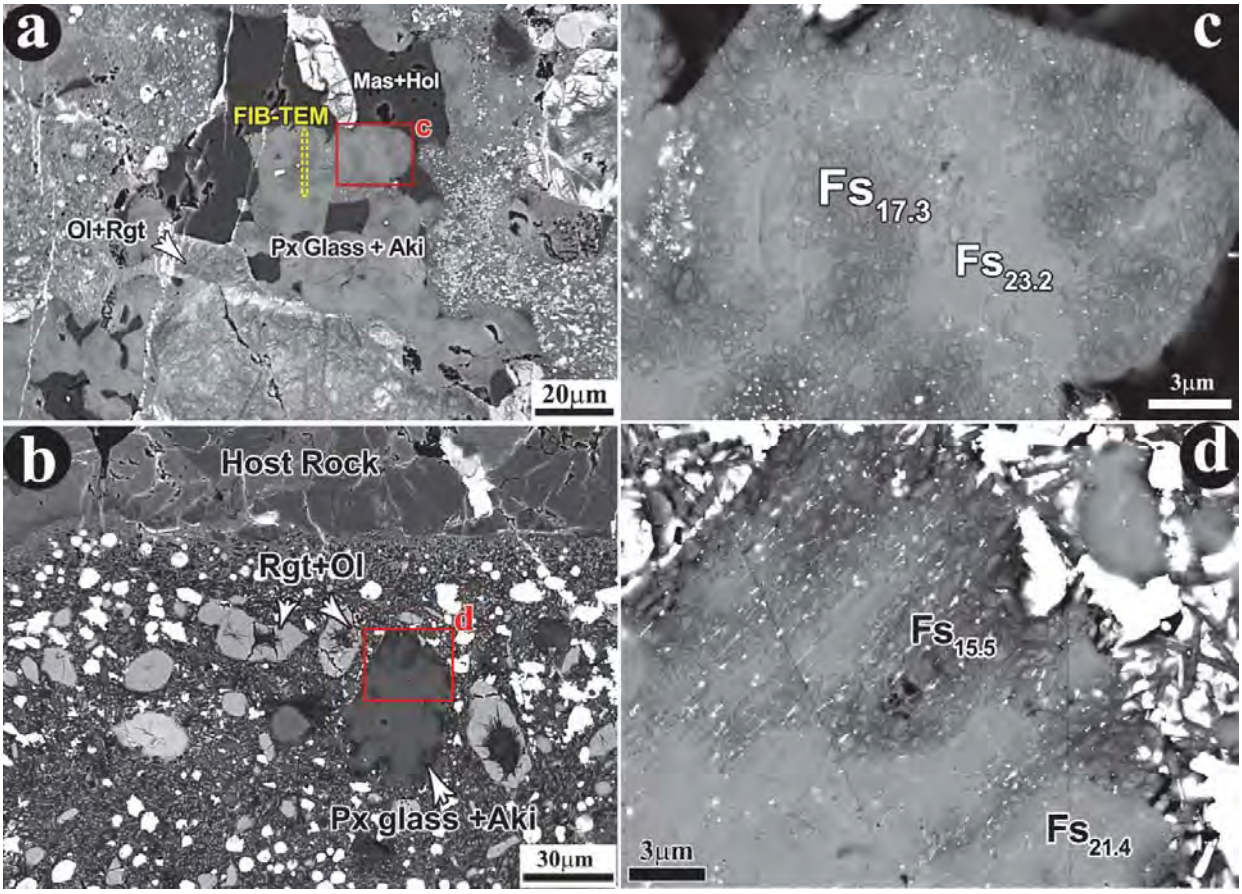

Fig. 2 By Feng et al.

This is a preprint, the final version is subject to change, of the American Mineralogist (MSA)
Cite as Authors (Year) Title. American Mineralogist, in press.
(DOI will not work until issue is live.) DOI: http://dx.doi.org/10.2138/am-2017-5905

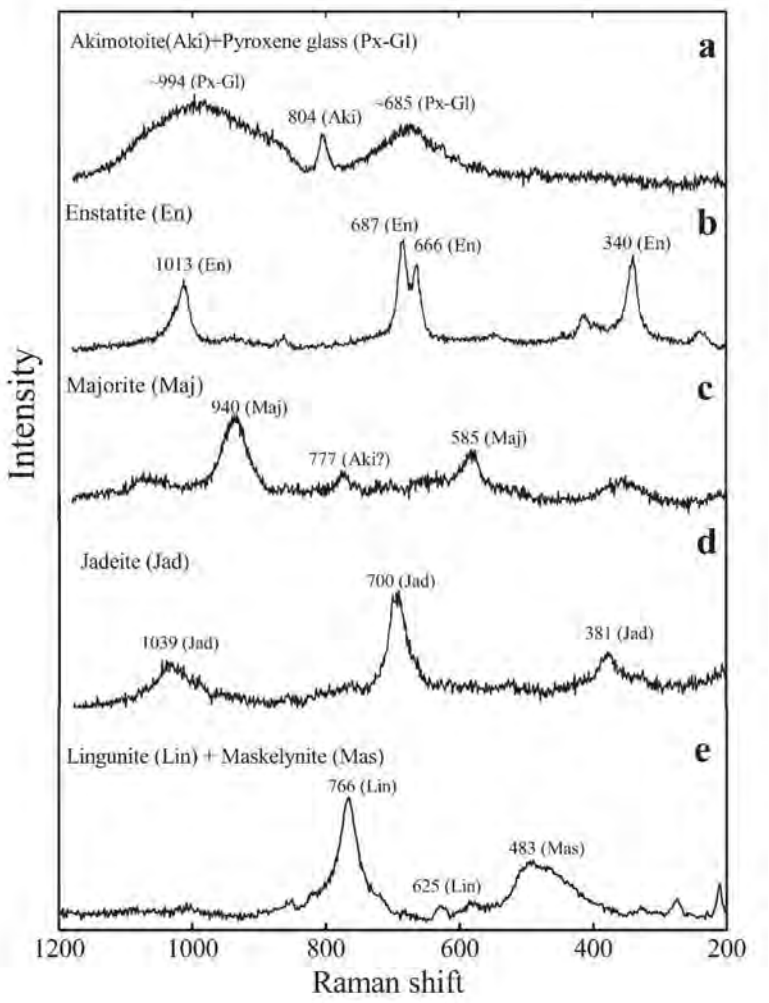

Fig. 3

By Feng et al.

This is a preprint, the final version is subject to change, of the American Mineralogist (MSA)
Cite as Authors (Year) Title. American Mineralogist, in press.
(DOI will not work until issue is live.) DOI: http://dx.doi.org/10.2138/am-2017-5905

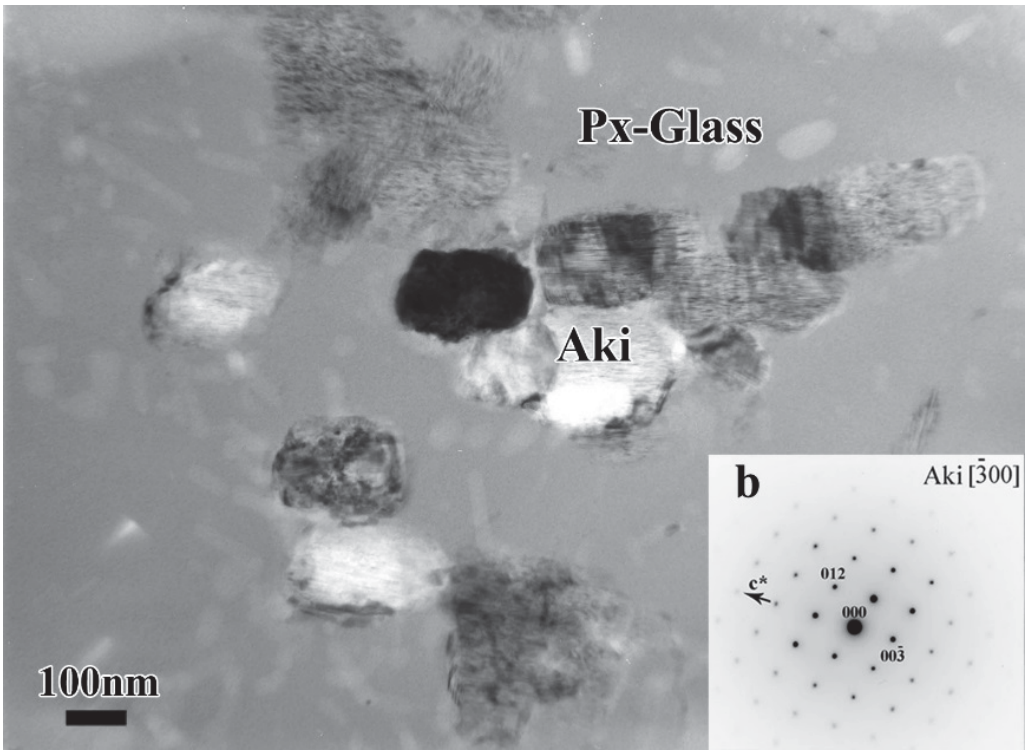

Fig. 4 By Feng et al.

This is a preprint, the final version is subject to change, of the American Mineralogist (MSA)
Cite as Authors (Year) Title. American Mineralogist, in press.
(DOI will not work until issue is live.) DOI: http://dx.doi.org/10.2138/am-2017-5905

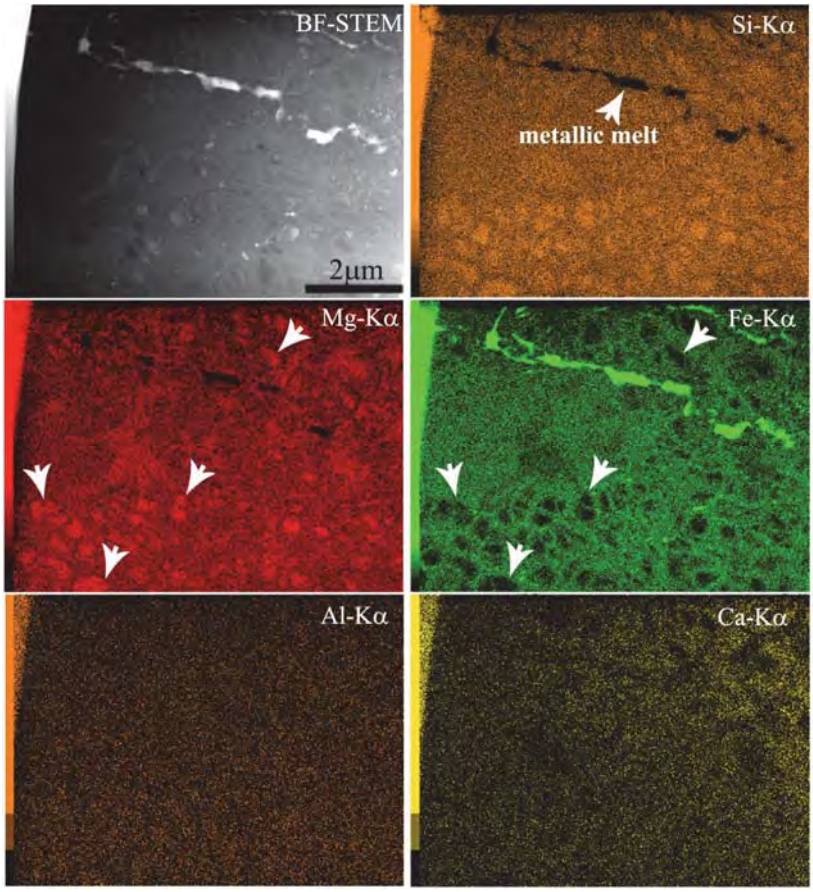

Fig. 5

By Feng et al.

This is a preprint, the final version is subject to change, of the American Mineralogist (MSA)
Cite as Authors (Year) Title. American Mineralogist, in press.
(DOI will not work until issue is live.) DOI: http://dx.doi.org/10.2138/am-2017-5905

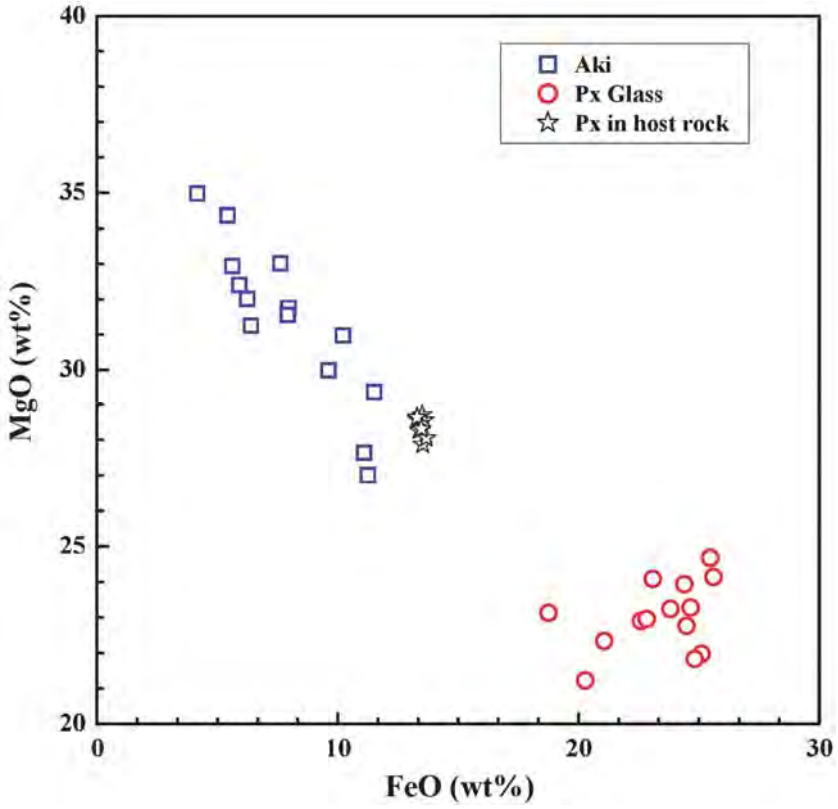

Fig. 6 By Feng et al.

This is a preprint, the final version is subject to change, of the American Mineralogist (MSA)
Cite as Authors (Year) Title. American Mineralogist, in press.
(DOI will not work until issue is live.) DOI: http://dx.doi.org/10.2138/am-2017-5905

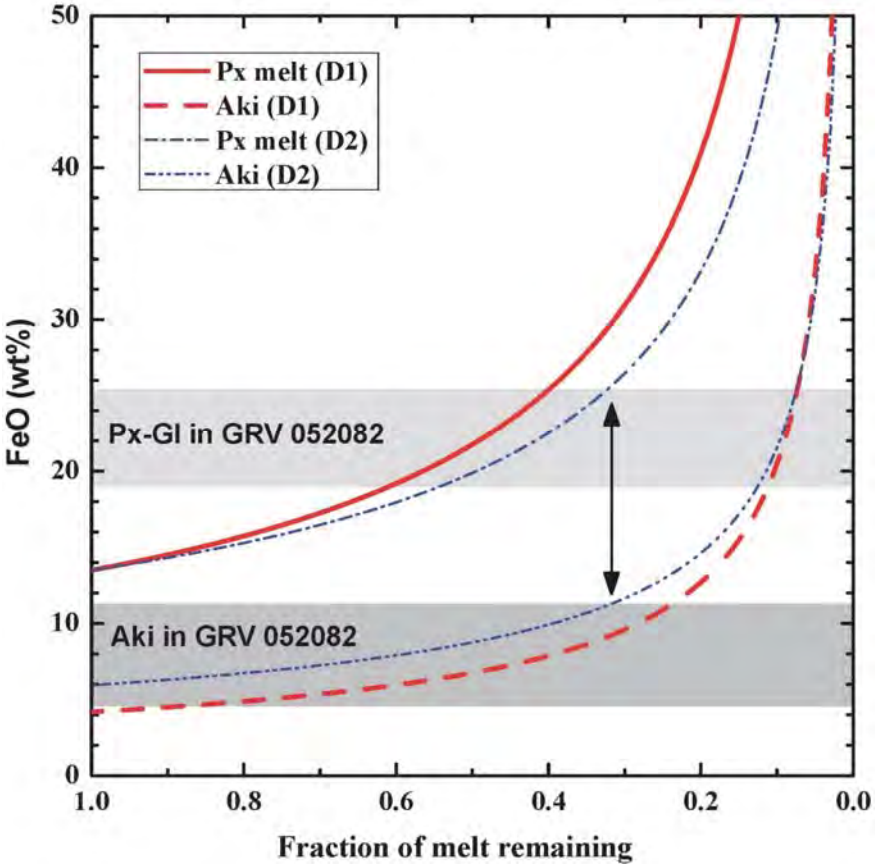

Fig. 7 By Feng et al.